ARTICLE

Typeset with jnst.cls <ver.2.1>

Reactor reactivity calculations with simplified-P_3 and perturbation theories

Jun-Shuang Fan[1]*, Go Chiba[2].

[1] *Division of Energy and Environmental System, Graduate School of Engineering, Hokkaido University, Kita 13 Nishi 8, Kita-ku, Sapporo, 060-8628, Japan.*

[2] *Division of Applied Quantum Science and Engineering, Faculty of Engineering, Hokkaido University.*

A new method to calculate reactivity of nuclear reactors through combining the simplified-P_3 (SP_3) and perturbation theories is proposed. The focus of this study is the sodium void reactivity calculations in the fast spectrum reactors. Verification of this new method was conducted with an OECD/NEA benchmark which contains four sodium-cooled fast reactors differing in fuel type and core size. Sodium void reactivity attribution analysis indicates that more accurate prediction of the scattering and leakage components of reactivity can be obtained with the new method compared to the diffusion-perturbation method, and that the computation time is reduced compared with the S_N-perturbation method. A term having an unclear physical meaning in the SP_3-perturbation method was investigated using a transformed SP_3 equation set which is different from the widely used form. Results suggested the equation derivation and code implementation are successful, and the new method shows obvious advantage in component-wise reactivity calculations.

Keywords: fast reactor, sodium void reactivity, simplified-P_3, perturbation theory

*Corresponding author. Email: fanjsh@eng.hokudai.ac.jp

Declaration of this AOM

1. Introduction

The Simplified-P_N (SP_N) theory was initially proposed by Gelbard[1] in 1960. Larsen et al.[2] concluded that although a solid theory basis was not constructed initially, the SP_N theory was proven valid through application.The SP_N theory can be regarded as an intermediate point between the transport theory and the diffusion theory. From the perspective of practice, the SP_3 theory has an obvious advantage since it could give more accurate results than the diffusion theory does with less computation burden compared with the transport theory, such as the spherical harmonic (P_N) method, the discrete ordinates (S_N) method and the method of characteristics. In the following decades, the theoretical basis of SP_N was gradually filled. Recently, a new and rigorous SP_N theory with rigorous interface and boundary conditions was built by Chao[3] in 2016. However, the conventional SP_N theory is still attractive to the nuclear engineering research community from the perspective of engineering practice. Research themes vary from GPU acceleration for reactor physics analysis[4], pin-wise homogenization treatment[5], variance reduction[6] and so on.

The perturbation theory, which originated from quantum science, was developed to evaluate the impact of perturbation (small disturbances) on systems. In the field of reactor engineering, there is a great concern about the impact of perturbation on a reactor system. Therefore, the perturbation theory has been widely used in reactor reactivity analyses. It is well known that reactivity can be calculated using two effective neutron multiplication factor (k_{eff}) values before and after perturbation, known as *direct calculation*. This, however, does not reveal the relationship between reactivity and physical quantities. Applying the perturbation theory, one the other hand, clarifies the contribution of each of the different physical quantities to reactivity. In the field of fast spectrum reactor analysis, reactivity can be categorized into different components: namely, yield, absorption, scattering and leakage components. The sum of yield, absorption, and scatter-

ing components is referred to as the non-leakage component. Component-wise reactivity information is crucial for fast reactor analysis due to the physical processes that it can reveal.

In the present work, a new method, which is referred to as the SP_3-Perturbation (SP_3P) method, has been developed for fast reactor reactivity analysis based on the SP_3 and perturbation theories. A term having unclear physical meaning is discussed since it complicates the categorization of reactivity. This difficulty was resolved using perturbation equations under the P_3 theory. P_3-Perturbation equations (P_3P) suggested that the term having unclear physical meaning in the SP_3P equations comes from math manipulation. The authors innovatively use a transformed SP_3 equation set which is different from the widely used form to give the perturbation expression under the SP_3 theory. To distinguish these two SP_3P methods, the authors label them SP_3P and Original-SP_3-Perturbation (OSP_3P) methods, respectively. The word *original* represents the SP_3 equations that are not manipulated to form diffusion-like equations. The method of OSP_3P can actually be regarded as a second version of SP_3P. Then, both methods were implemented into CBZ, which is a general-purpose deterministic reactor physics analysis code system[9]. Verification of the new method was carried out with an OECD/NEA fast reactor benchmark[7]. The rationale for choosing this benchmark was that four sodium-cooled fast reactor concepts which differ in fuel type and core size are provided. It is believed that these four concepts could represent the general type of sodium-cooled fast reactors. Finally, the merit of the SP_3P method compared with the diffusion method was investigated using a designed void pattern problem.

The reminder of this paper is structured as follows: In Section 2, details of the SP_3P method derivation and code implementation are introduced as a theoretical background. A term having unclear physical meaning from the perspective of component-wise reactivity is also discussed in this section. The numerical calculation for verification and the advantage

for investigation are introduced and discussed in Section 3. Conclusion is discussed in Section 4.

2. Theory and implementation

2.1. Perturbation theory and component-wise reactivity

Reactivity (coefficient) calculation is a crucial part of reactor physics analysis from the perspective of reactor transient safety and control. There is a need of decomposing the reactivity to clarify the relevant physical processes. A classical method is using the perturbation theory for reactivity calculation. Therefore, the perturbation theory and reactivity categorization are explained in this section.

The discretized neutron transport equation (and its approximation form) can be expressed in a matrix form,

$$\boldsymbol{A}\phi = \frac{1}{k_{\text{eff}}}\boldsymbol{F}\phi, \tag{1}$$

in which

$\boldsymbol{A}$: operator for neutron loss,
$\boldsymbol{F}$: operator for neutron generation by fission reaction, and
ϕ : vector representing neutron flux.

The adjoint neutron transport equations can be obtained by simply transposing the operators. The perturbation theory requires the adjoint matrix $\boldsymbol{A}^{\dagger}$ (which could also be written as $\boldsymbol{A}^{H}$ or $\boldsymbol{A}^{*}$, representing the Hermite transpose), and it is actually the conjugate transposition matrix of $\boldsymbol{A}$. The conjugate transposition matrix of $\boldsymbol{A}$ is identical to its transposition matrix $\boldsymbol{A}^{T}$ in reactor physics calculation since all parameters are real numbers.

Reactivity $\Delta\rho$ can be calculated with the following equation according to the perturbation theory,

$$\Delta\rho = \frac{\frac{1}{k}\left\langle \phi^{\dagger}, \Delta\boldsymbol{F}\phi' \right\rangle - \left\langle \phi^{\dagger}, \Delta\boldsymbol{A}\phi' \right\rangle}{\left\langle \phi^{\dagger}, \boldsymbol{F}'\phi' \right\rangle}, \tag{2}$$

in which

ϕ' : neutron flux after perturbation,
$\phi^\dagger$: adjoint neutron flux,
$\langle\rangle$: integrating for all spaces,
$\Delta \boldsymbol{F}, \Delta \boldsymbol{A}$: changes in operators A and F after perturbation, and
$\boldsymbol{A}', \boldsymbol{F}'$: operators A and F after perturbation.

Typically, reactivity can be divided into four parts: yield, absorption, scattering, and leakage components, in which the sum of the yield, absorption and scattering components is regarded as the non-leakage component. This categorization is general in reactivity analysis. Given that the problem under study is the coolant loss (sodium void) reactivity in fast spectrum reactors, another categorization specified for fast reactor reactivity analysis is introduced here. Four phenomena[8] contribute to the overall sodium void reactivity; they are (1) spectral hardening, (2) increased leakage, (3) eliminated sodium capture, and (4) change in self-shielding. These can be viewed as a categorization of the sodium void reactivity. The correspondence between these two categorizations are explained as follows.

In the first categorization, the $\nu\Sigma_f$-perturbation reactivity and χ-perturbation reactivity are regarded as the yield component; the Σ_a-perturbation reactivity is categorized as the absorption component; the $\Sigma_{s,g\to g'}$-perturbation reactivity is categorized as the scattering component; and the diffusion coefficient D-perturbation reactivity (in the case of theories with the diffusion approximation) is categorized as the leakage component. Note that the notations used here are classical and defined later.

Table 1 lists the general categorization of sodium void reactivity with examples of expression. The actual categorization corresponding to the SP_3P method implemented into CBZ is slightly different from this table since there are two neutron fluxes and two adjoint neutron fluxes in the SP_3P equations. The ϕ^2 is the second-order Legendre expansion moment of angular neutron flux. Higher-order Legendre moments of angular flux are considered to be related to neutron leakage. Therefore, the reactivity described by both $\phi^{2\dagger}$ and ϕ^2 is categorized as leakage component in the present work.

It is necessary to emphasize here that there is a clear corresponding relationship

Table 1 Information about reactivity categorization in the present work.

Component	Causes	Expression example
Yield	$\nu\Sigma_f$ and χ	$\left\langle \phi^\dagger, \Delta\Sigma_f\phi' \right\rangle$
Absorption	Σ_a	$\left\langle \phi^\dagger, \Delta\Sigma_a\phi' \right\rangle$
Scattering	$\Sigma_{s,g\to g'}$	$\left\langle (\phi^\dagger_{g'} - \phi^\dagger_g), \Delta\Sigma_{s,g'\to g}\phi'_{g'} \right\rangle$
Leakage	Diffusion coefficient D	$\left\langle \nabla\phi^\dagger, \Delta D\nabla\phi' \right\rangle$

between the two categorizations mentioned above. The spectral hardening component corresponds exactly to the scattering component; the increased leakage component corresponds to the leakage component; the elimination of neutron capture by sodium and change in self-shielding components together correspond to the absorption and yield components[8], respectively. Considering the clear corresponding relationship, therefore, the general method of categorization was accepted in the present work.

2.2. Derivation of SP_3-Perturbation (SP_3P) equation

This work starts with derivation of perturbation equations of the SP_3 theory. The SP_3 equations with isotropic scattering source can be expressed as shown below, according to the works of Larsen et al.[2], Tatsumi and Yamamoto[10]:

$$-D_g\nabla^2\left(\phi^0_g + 2\phi^2_g\right) + \Sigma_{r,g}\left(\phi^0_g + 2\phi^2_g\right) = \frac{\chi_g}{k_{\text{eff}}}\sum_{g'=1}^{G}\nu\Sigma_{f,g'}\phi^0_{g'} + \sum_{g'\neq g}^{G}\Sigma^0_{s,g'\to g}\phi^0_{g'} + 2\Sigma_{r,g}\phi^2_g, \tag{3}$$

$$-\frac{27}{35}D_g\nabla^2\phi^2_g + \Sigma_{t,g}\phi^2_g = \frac{2}{5}\left\{\Sigma_{r,g}\phi^0_g - \left(\frac{\chi_g}{k_{\text{eff}}}\sum_{g'=1}^{G}\nu\Sigma_{f,g'}\phi^0_{g'} + \sum_{g'\neq g}^{G}\Sigma^0_{s,g'\to g}\phi^0_{g'}\right)\right\}, \tag{4}$$

where

D_g : diffusion coefficient of group g,
ϕ^l_g : neutron flux of l-th order in group g,
$\Sigma_{r,g}$: removal cross-section in group g,
χ_g : neutron fission spectrum in group g,
$\Sigma^l_{s,g'\to g}$: l-th order macroscopic scattering cross-section from group g' to g,
G : the number of energy groups.

Then, we write the SP_3 equations set into an operator form and obtaining the adjoint

SP_3 equations set,

$$-D_g\nabla^2\phi_g^{0\dagger}+\Sigma_{r,g}(\phi_g^{0\dagger}-\frac{2}{5}\phi_g^{2\dagger})-\sum_{g'\neq g}^{G}\left[\Sigma_{s,g\to g'}^{0}(\phi_{g'}^{0\dagger}-\frac{2}{5}\phi_{g'}^{2\dagger})\right]=\frac{1}{k}\nu\Sigma_{f,g}\sum_{g'=1}^{G}\chi_{g'}(\phi_{g'}^{0\dagger}-\frac{2}{5}\phi_{g'}^{2\dagger}), \tag{5}$$

$$-D_g\nabla^2(2\phi_g^{0\dagger}+\frac{27}{35}\phi_g^{2\dagger})+\Sigma_{t,g}\phi_g^{2\dagger}=0, \tag{6}$$

in which $\phi_g^{l\dagger}$ is l-th order adjoint neutron flux in group g.

Adjoint neutron flux $\phi^\dagger$ is used as a weight in reactivity calculations. Splitting the Eq. (2) and integrating only over energy groups, then $(\phi^\dagger,\Delta A\phi')_{\text{energy}}$ and $(\phi^\dagger,\Delta F\phi')_{\text{energy}}$, are expressed by Eqs. (7) and (8). Please note that here we assume the fission spectrum χ is not affected by perturbation for simplification. Taking the perturbation of χ into account, we can add $\Delta\chi_g$ term into Eq. (8).

$$\begin{aligned}(\phi^\dagger,\Delta A\phi')_{\text{energy}}=\sum_{g=1}^{G}\Bigg\{&\phi_g^{0\dagger}\left[(-\Delta D_g\nabla^2+\Delta\Sigma_{r,g})\phi_g^{\prime 0}-2\Delta D_g\nabla^2\phi_g^{\prime 2}-\sum_{g'\neq g}^{G}\Delta\Sigma_{s,g'\to g}^{0}\phi_{g'}^{\prime 0}\right]\\&+\phi_g^{2\dagger}\left[-\frac{2}{5}\Delta\Sigma_{r,g}\phi_g^{\prime 0}-(\frac{27}{35}\Delta D_g\nabla^2-\Delta\Sigma_{t,g})\phi_g^{\prime 2}+\frac{2}{5}\sum_{g'\neq g}^{G}\Delta\Sigma_{s,g'\to g}^{0}\phi_{g'}^{\prime 0}\right]\Bigg\},\end{aligned} \tag{7}$$

$$(\phi^\dagger,\Delta F\phi')_{\text{energy}}=\sum_{g=1}^{G}\left(\phi_g^{0\dagger}\chi_g\sum_{g'=1}^{G}\Delta\nu\Sigma_{f,g'}\phi_{g'}^{\prime 0}\right). \tag{8}$$

The form of Eq.(7) can be modified according to the definition of component-wise reactivity. Among these, the most important one is scattering component reactivity since the expression considering the removal cross-section is

$$\Sigma_{r,g}=\Sigma_{a,g}+\sum_{g'\neq g}^{G}\Delta\Sigma_{s,g\to g'}-\Sigma_{n2n,g}. \tag{9}$$

Scattering component reactivity in the SP_3P method can be expressed as Eq. (10) based on the general way of categorization,

$$(\phi^\dagger,\Delta A\phi')_{scat,\text{energy}}=\sum_{g=1}^{G}\sum_{g'=1}^{G}(\phi_{g'}^{0\dagger}-\phi_g^{0\dagger})\Delta\Sigma_{s,g'\to g}^{0}\phi_{g'}^{\prime 0}-\frac{2}{5}\sum_{g=1}^{G}\sum_{g'=1}^{G}(\phi_{g'}^{2\dagger}-\phi_g^{2\dagger})\Delta\Sigma_{s,g'\to g}^{0}\phi_{g'}^{\prime 0}. \tag{10}$$

It is notable that the physical meaning of the second term of the right-hand-side of Eq. (10), $-\frac{2}{5}(\phi_{g'}^{2\dagger}-\phi_g^{2\dagger})\Delta\Sigma_{s,g'\to g}^0\phi_{g'}^{\prime 0}$, is not as clear as the first term. The physical interpretation of ϕ^2 is clear since it comes from the Legendre polynomials expansion of the angular neutron flux in the transport equation. The higher-order Legendre expansion moment is considered to be related to neutron leakage as mentioned previously. A straightforward interpretation of the physical meaning of this term is that $\phi^{2\dagger}$ is used as a weight function to evaluate the reactivity caused by perturbation of Σ_r. However, categorizing this term presents a challenge.

From the perspective of angular neutron flux $\phi^{2\dagger}$, the $-\frac{2}{5}(\phi_{g'}^{2\dagger}-\phi_g^{2\dagger})\Delta\Sigma_{s,g'\to g}\phi_{g'}^{\prime 0}$ term should be categorized as the leakage component. According to the calculation result shown in Section 3, however, this term should be categorized as the scattering component reactivity. This confusing fact promoted the authors to trace the source of this part of reactivity through comparison with the P_3-perturbation equations. This is summarized in the next section.

2.3. Derivation of OSP$_3$-Perturbation (OSP$_3$P) method

The SP$_3$P method was implemented into the CBZ code system. The numerical calculation result implies a fact that the $-\frac{2}{5}(\phi_{g'}^{2\dagger}-\phi_g^{2\dagger})\Delta\Sigma_{s,g'\to g}\phi_{g'}^{\prime 0}$ term belongs to the scattering component since the result on the scattering component given by the SP$_3$P method was more accurate if this term were counted. To give theoretical explanation, further investigation was carried out using the P_N-perturbation since the SP$_N$ theory originated from the P_N theory.

The P_3 equation set of one-dimensional planar system is expressed as

$$\frac{d}{dx}\phi_g^1+\Sigma_{r,g}\phi_g^0-\sum_{g'\neq g}^{G}\Sigma_{s,g'\to g}^0\phi_{g'}^0=\frac{\chi_g}{k_{\text{eff}}}\sum_{g'=1}^{G}\nu\Sigma_{f,g'}\phi_{g'}^0, \tag{11}$$

$$\frac{1}{3}\frac{d}{dx}\phi_g^0+\frac{2}{3}\frac{d}{dx}\phi_g^2+\Sigma_{t,g}\phi_g^1-\sum_{g'=1}^{G}\Sigma_{s,g'\to g}^1\phi_{g'}^1=0, \tag{12}$$

$$\frac{2}{5}\frac{d}{dx}\phi_g^1 + \frac{3}{5}\frac{d}{dx}\phi_g^3 + \Sigma_{t,g}\phi_g^2 - \sum_{g'=1}^{G}\Sigma_{s,g'\to g}^2\phi_{g'}^2 = 0, \tag{13}$$

$$\frac{3}{7}\frac{d}{dx}\phi_g^2 + \Sigma_{t,g}\phi_g^3 - \sum_{g'=1}^{G}\Sigma_{s,g'\to g}^3\phi_{g'}^3 = 0. \tag{14}$$

In Gelbard's work[1], the SP_3 equations are derived by replacing the one-dimensional operator with multi-dimensional operator ∇. The subsequent derivations included in the present paper used the same expression to keep consistency. Besides, the second- and higher-order scattering moments are generally ignored, i.e., $\Sigma_s^l \approx 0, (l \geq 2)$. The higher-order scattering terms in equations (13) and (14) are retained for consistency with the other equations. Then, we introduce the widely used *out-scatter approximation* for the odd-order moment which is used to get the transport cross-section[11],

$$\sum_{g'=1}^{G}\Sigma_{s,g'\to g}^N\phi_{g'}^N \approx \sum_{g'=1}^{G}\Sigma_{s,g\to g'}^N\phi_g^N, (N = 1, 3, 5, ...), \tag{15}$$

and after straightforward derivation, a transformed SP_3 equations set can be obtained as

$$-D_g\nabla^2(\phi_g^0 + 2\phi_g^2) + \Sigma_{r,g}\phi_g^0 - \sum_{g'\neq g}^{G}\Sigma_{s,g'\to g}^0\phi_{g'}^0 = \frac{\chi_g}{k_{\text{eff}}}\sum_{g'=1}^{G}\nu\Sigma_{f,g'}\phi_{g'}^0, \tag{16}$$

$$-\frac{2}{5}D_g\nabla^2(\phi_g^0 + 2\phi_g^2) - \frac{3}{5}D_g^{'}\nabla^2\phi_g^2 + \Sigma_{t,g}\phi_g^2 - \sum_{g'=1}^{G}\Sigma_{s,g'\to g}^2\phi_{g'}^2 = 0, \tag{17}$$

in which

$$D_g = \frac{1}{3(\Sigma_{t,g} - \sum\limits_{g'=1}^{G}\Sigma_{s,g\to g'}^1)}, \tag{18}$$

$$D_g^{'} = \frac{3}{7(\Sigma_{t,g} - \sum\limits_{g'=1}^{G}\Sigma_{s,g\to g'}^3)}. \tag{19}$$

The authors called this transformed SP_3 equations as original-SP_3 (OSP_3) equations since they are derived from the P_3 equations straightforwardly.

The expression of Eq. (19) is not as common as Eq. (18) which is the definition of the diffusion coefficient. Assuming that the third-order scattering moment is approximately equal to the first-order scattering moment, which can be described by $\sum\limits_{g'=1}^{G}\Sigma_{s,g\to g'}^1 =$

$\sum_{g'=1}^{G} \Sigma^3_{s,g\to g'}$, the following relation holds,

$$D_g^{'} = \frac{3 \cdot 3}{7 \cdot 3(\Sigma_{t,g} - \sum_{g'=1}^{G} \Sigma^3_{s,g\to g'})} \approx \frac{9}{7} D_g.$$

It is necessary to clarify here that $\frac{3}{5} D_g^{'}$ in Eq. (17) is exactly the second-order moment diffusion coefficient D_g^2 in the widely used form of SP_3 equations[10], and these two notations both represent $\frac{27}{35} D_g$. The assumption above can be derived by the previous works[2,10]. Then, the OSP_3 equations can be written in exactly the same form as the SP_3 equations by assuming that $\sum_{g'} \Sigma^2_{s,g'\to g} \phi^2_{g'} \approx 0$, which is another general assumption[2].

With the approximations mentioned above, Eqs. (16) and (17) are equivalent to Eqs. (3) and (4). Their adjoint equations, however, are not equivalent. This means that although neutron fluxes ϕ^0 and ϕ^2 described by SP_3 and OSP_3 are identical, their adjoint neutron fluxes, $\phi^{0\dagger}$ and $\phi^{2\dagger}$, are not identical. As described in Section 2.1, the adjoint equations are obtained by transposing the operators $\boldsymbol{A}$ and $\boldsymbol{F}$. Equations (5) and (6) are adjoint equations for SP_3. For OSP_3, the adjoint equations are

$$- D_g \nabla^2 \phi_g^{0\dagger} - \frac{2}{5} D_g \nabla^2 \phi_g^{2\dagger} + \Sigma_{r,g} \phi_g^{0\dagger} - \sum_{g'\neq g} \Sigma^0_{s,g\to g'} \phi^{0\dagger}_{g'} = \frac{1}{k} \nu\Sigma_{f,g} \sum_{g'=0}^{G} \chi_{g'} \phi^{0\dagger}_{g'}, \tag{20}$$

$$- 2D_g \nabla^2 \left(\phi_g^{0\dagger} + \frac{2}{5} \phi_g^{2\dagger} \right) - \frac{3}{5} D_g^{'} \nabla^2 \phi_g^{2\dagger} + \Sigma_{t,g} \phi_g^{2\dagger} - \sum_{g'\neq g} \Sigma^2_{s,g\to g'} \phi^{2\dagger}_{g'} = 0. \tag{21}$$

Following the same derivation process, one can obtain the perturbation equations based on OSP_3 for reactivity calculation. The specific expression of the OSP_3-perturbation is shown here, in the same form as Eqs. (7) and (8),

$$\begin{aligned}(\phi^\dagger, \Delta A \phi')_{\text{energy}} = \sum_{g=1}^{G} \Bigg\{ & \phi_g^{0\dagger} \left[(-\Delta D_g \nabla^2 + \Delta\Sigma_{r,g}) \phi_g^{0'} - 2\Delta D_g \nabla^2 \phi_g^{2'} - \sum_{g'\neq g} \Delta\Sigma^0_{s,g'\to g} \phi^{0'}_{g'} \right] \\ & + \phi_g^{2\dagger} \left[-\frac{2}{5} \Delta D_g \nabla^2 \phi_g^{0'} + (\Delta\Sigma_{r,g} - \frac{4}{5} \Delta D_g \nabla^2 - \frac{3}{5} \Delta D_g^{'} \nabla^2) \phi_g^{2'} \right] \Bigg\},\end{aligned} \tag{22}$$

$$(\phi^\dagger, \Delta F \phi')_{\text{energy}} = \sum_{g=1}^{G} \left(\phi_g^{0\dagger} \chi_g \sum_{g'=1}^{G} \Delta\nu\Sigma_{f,g'} \phi^{\prime 0}_{g'} \right). \tag{23}$$

An important fact observed from Eq. (22) is that there is no such $(\phi^{2\dagger}_{g'} - \phi^{2\dagger}_{g}), \Delta\Sigma^{0}_{s,g'\to g}\phi^{0}_{g'}$ term. The scattering component reactivity in the OSP_3P method only has

$$(\phi^{\dagger}, \Delta A\phi')_{scat,\text{energy}} = \sum_{g=1}^{G}\sum_{g'=1}^{G}(\phi^{0\dagger}_{g'} - \phi^{0\dagger}_{g})\Delta\Sigma^{0}_{s,g'\to g}\phi'^{0}_{g'}. \tag{24}$$

This discovery indicates the term having unclear physical meaning in the SP_3P method occurs due to math manipulation. Using OSP_3P can avoid the difficulty in categorizing reactivity since each term in OSP_3P implies certain physical meaning.

2.4. Implementation into the CBZ code system

The work to achieve the SP_3P and OSP_3P functions includes two parts,

(a) implementation of adjoint neutron flux $\phi^{\dagger}$ calculation functions, and

(b) implementation of perturbation calculation function according to the corresponding equations.

The first part of this work is to obtain forward neutron flux, adjoint neutron flux, and eigenvalue. The forward neutron flux given by the SP_3 and OSP_3 equations is identical since these two equation sets are equivalent. Therefore, the SP_3 forward calculation function can be used for the OSP_3P calculation, which means it is not necessary to implement the OSP_3 forward calculation function. The form of equations implemented into CBZ should be changed into a diffusion-like form,

$$-D\nabla^2 f + \Sigma f = S.$$

This is because the diffusion-like form is a numerically solvable form, and the diffusion-like form equation can be implemented with an existing diffusion solver module. The

diffusion-like form of the SP_3 forward equation set is

$$-D_g\nabla^2\left(\phi_g^0+2\phi_g^2\right)+\Sigma_{r,g}\left(\phi_g^0+2\phi_g^2\right)= \frac{\chi_g}{k_{\text{eff}}}\sum_{g'=1}^{G}\nu\Sigma_{f,g'}\phi_{g'}^0+\sum_{g'\neq g}^{G}\Sigma_{s,g'\to g}\phi_{g'}^0+2\Sigma_{r,g}\phi_g^2, \tag{25}$$

$$-\frac{27}{35}D_g\nabla^2\phi_g^2+(\Sigma_{t,g}+\frac{4}{5}\Sigma_{r,g})\phi_g^2= \frac{2}{5}\left\{\Sigma_{r,g}(\phi_g^0+2\phi_g^2)-\left(\frac{\chi_g}{k_{\text{eff}}}\sum_{g'=1}^{G}\nu\Sigma_{f,g'}\phi_{g'}^0+\sum_{g'\neq g}^{G}\Sigma_{s,g'\to g}\phi_{g'}^0\right)\right\}. \tag{26}$$

The diffusion-like form of the SP_3 adjoint equation set is

$$-D_g\nabla^2(\phi_g^{0\dagger}+\phi_g^{2\dagger})+\Sigma_{r,g}(\phi_g^{0\dagger}+\phi_g^{2\dagger})= \frac{1}{k_{\text{eff}}}\nu\Sigma_{f,g}\sum_{g'=1}^{G}\chi_{g'}(\phi_{g'}^{0\dagger}+\phi_{g'}^{2\dagger})+\sum_{g'\neq g}^{G}\left[\Sigma_{s,g\to g'}(\phi_{g'}^{0\dagger}+\phi_{g'}^{2\dagger})\right]-2D_g\nabla^2\phi_g^{2\dagger}, \tag{27}$$

$$-\frac{27}{35}D_g\nabla^2(-\frac{28}{27}\phi_g^{0\dagger}+\phi_g^{2\dagger})+\Sigma_{t,g}\left(-\frac{28}{27}\phi_g^{0\dagger}+\phi_g^{2\dagger}\right)=-\frac{28}{27}\Sigma_{t,g}\phi_g^{0\dagger}. \tag{28}$$

The diffusion-like form of the OSP_3 adjoint equation set is

$$-D_g\nabla^2\left(\phi_g^{0\dagger}+\frac{2}{5}\phi_g^{2\dagger}\right)+\Sigma_{r,g}\left(\phi_g^{0\dagger}+\frac{2}{5}\phi_g^{2\dagger}\right)= \frac{1}{k_{\text{eff}}}\nu\Sigma_{f,g}\sum_{g'=1}^{G}\chi_{g'}\phi_{g'}^{0\dagger}+\sum_{g'\neq g}^{G}\Sigma_{s,g\to g'}^{0}\phi_{g'}^{0\dagger}+\frac{2}{5}\Sigma_{r,g}\phi_g^{2\dagger}, \tag{29}$$

$$-2D_g\nabla^2\left(\phi_g^{0\dagger}+\frac{7}{10}\phi_g^{2\dagger}\right)+\frac{10}{3}\Sigma_{t,g}\left(\phi_g^{0\dagger}+\frac{7}{10}\phi_g^{2\dagger}\right)=\frac{10}{3}\Sigma_{t,g}\left(\phi_g^{0\dagger}+\frac{2}{5}\phi_g^{2\dagger}\right). \tag{30}$$

After these three coupled equation set calculation functions are implemented into CBZ, the perturbation reactivity calculation function is implemented separately for the yield, absorption, scattering, and leakage components, respectively. Due to the high similarity of the SP_3P and OSP_3P equations, the implementation of OSP_3P can be carried out with minor modifications based on the SP_3P method.

3. Numerical calculation and result analysis

3.1. Numerical calculation information

An OECD/NEA fast reactor benchmark report[7] is used in this work. Four different sodium-cooled fast reactors that differ in core size and fuel type are described in this benchmark. It is believed that they can represent the general type of fast reactors. Basic information for these four reactors is shown in Table 2. MET-1000 and MOX-1000 are middle-sized cores, and MOX-3600 and CAR-3600 are large-sized cores. They use metallic fuel, MOX fuel, and carbide fuel, respectively.

Table 2 Fuel type and core size information for each benchmark core

Core name	Fuel type	Power level [MWe]
MET-1000	Metallic	1,000
MOX-1000	MOX	1,000
MOX-3600	MOX	3,600
CAR-3600	Carbide	3,600

CBZ applies the classic *two-step method* in reactor physics calculation and multiple methodologies are available. The calculation methodology chosen for this work was the two-dimensional lattice model (in lattice calculation step) with a 70-group structure "JAERI fast set-3 (JFS-3)" that was proposed by JAERI (presently JAEA) for sodium-cooled fast reactor analysis. The multi-group constant is generated by CBZ based on the JENDL-4.0 library. As for the whole-core calculation step, the core is modeled as a two-dimensional multi-layer cylinder geometry. The perturbation condition (void patterns) for sodium void reactivity calculation assumes that (1) all sodium in core is lost and (2) sodium in some layers is lost. The second void pattern is called a *local void pattern* in this work.

The reliability of CBZ on fast reactor analysis has been verified by one of our previous works[12], and details such as modeling and methodology were systematically discussed. The result calculated by a transport solver (S_N method) in CBZ is regarded as the reference in the current work, and is compared with the results of SP_3P and OSP_3P method

calculations in the next section. In FRBurner, the order of the transport solver is determined by two parameters: P_N and S_N, which are the maximum order of the Legendre polynomial for the anisotropic scattering cross-section expansion and the order of discrete ordinates method, respectively. It is notable that this P_N-order here is different from the P_N method. In present work, the order of transport solver is P_1S_4.

Since the result given by perturbation calculation must be identical to the direct calculation result theoretically, it is necessary to compare the perturbation calculation result with the direct calculation result to confirm the validity. Reactivity evaluated by direct calculation is given by two k_{eff} values before and after the perturbation,

$$\Delta\rho = \frac{1}{k_{\text{eff}}} - \frac{1}{k'_{\text{eff}}}. \tag{31}$$

The reactivity value should be unique no matter what method is applied.

3.2. Whole-core void pattern

At first, the whole-core void pattern is discussed. This void pattern is also discussed in the benchmark[7]. All sodium in the core is voided (with the exception of bond sodium inside fuel). Tables 3 to 6 exhibit the component-wise reactivity results given by the S_NP, OSP_3P, SP_3P and diffusion-perturbation (DP) methods for the four reactors, respectively. The relative percent difference (RPD) of the results given by the OSP_3P, SP_3P and DP methods compared with the S_NP method is also listed in these tables. The direct calculation results of the SP_3 and OSP_3 solvers in CBZ are included to prove validity. For the S_NP method, the yield, absorption, scattering, non-leakage and leakage component reactivity, and the net reactivity are shown in the tables. Specifically, the scattering component is separated into two parts, $\phi^{0\dagger}$ and $\phi^{2\dagger}$, for the OSP_3P and SP_3P methods. Table 7 presents the normalized computation time in second for each method in the MET-1000 problem calculation to show the magnitude of computation burden reduction.

Firstly, we could confirm the successful development of SP_3P and OSP_3P since the

Table 3 Verification and comparison of OSP_3P and OSP_3P functions for reactivity calculation (unit: pcm), MET-1000.

	Yield	Absorption	Scattering			Non-leakage	Leakage	Net	
S_NP	-14	221	3922			4129	-1812	2317	
	Yield	Absorption	Scattering	$\phi^{0\dagger}$ Scat	$\phi^{2\dagger}$ Scat	Non-leakage	Leakage	Net	Direct
OSP_3P	-14	222	3922	3922	-	4129	-1734	2396	2395
SP_3P	-14	222	3922	3816	105	4129	-1734	2396	2395
DP	-14	222	3902	-	-	4111	-1843	2268	-
RPD_OSP_3P	-0.70%	0.29%	-0.01%			0.01%	-4.33%	3.40%	
RPD_SP_3P	-0.70%	0.29%	-0.01%			0.01%	-4.33%	3.40%	
RPD_DP	1.89%	0.53%	-0.49%			-0.45%	1.68%	-2.11%	

* Net value and direct calculation result for OSP_3P/SP_3P method are 2395.6 and 2395.3, respectively.

Table 4 Verification and comparison of OSP_3P and OSP_3P functions for reactivity calculation (unit: pcm), MOX-1000.

	Yield	Absorption	Scattering			Non-leakage	Leakage	Net	
S_NP	-25	434	2970			3380	-1215	2165	
	Yield	Absorption	Scattering	$\phi^{0\dagger}$ Scat	$\phi^{2\dagger}$ Scat	Non-leakage	Leakage	Net	Direct
OSP_3P	-25	440	2965	2965	-	3381	-1166	2215	2215
SP_3P	-25	440	2965	2907	58	3381	-1166	2215	2215
DP	-25	441	2954	-	-	3370	-1214	2156	-
RPD_OSP_3P	0.04%	1.25%	-0.15%			0.03%	-4.08%	2.34%	
RPD_SP_3P	0.04%	1.25%	-0.15%			0.03%	-4.08%	2.34%	
RPD_DP	1.58%	1.47%	-0.54%			-0.30%	-0.08%	-0.42%	

Table 5 Verification and comparison of OSP_3P and OSP_3P functions for reactivity calculation (unit: pcm), MOX-3600.

	Yield	Absorption	Scattering			Non-leakage	Leakage	Net	
S_NP	-19	439	2441			2861	-662	2199	
	Yield	Absorption	Scattering	$\phi^{0\dagger}$ Scat	$\phi^{2\dagger}$ Scat	Non-leakage	Leakage	Net	Direct
OSP_3P	-19	445	2435	2435	-	2861	-626	2235	2235
SP_3P	-19	445	2435	2399	36	2861	-626	2235	2235
DP	-20	445	2428	-	-	2853	-646	2207	-
RPD_OSP_3P	-0.37%	1.33%	-0.25%			0.00%	-5.40%	1.62%	
RPD_SP_3P	-0.37%	1.33%	-0.25%			0.00%	-5.40%	1.62%	
RPD_DP	4.71%	1.40%	-0.55%			-0.29%	-2.43%	0.36%	

Table 6 Verification and comparison of OSP_3P and OSP_3P functions for reactivity calculation (unit: pcm), CAR-3600.

	Yield	Absorption	Scat			Non-leakage	Leakage	Net	
S_NP	-21	499	2867			3345	-871	2473	
	Yield	Absorption	Scattering	$\phi^{0\dagger}$ Scat	$\phi^{2\dagger}$ Scat	Non-leakage	Leakage	Net	Direct
OSP3	-21	509	2855	2855	-	3343	-831	2513	2513
SP3	-21	509	2855	2807	48	3343	-831	2513	2513
Diffusion	-21	510	2849	-	-	3338	-858	2481	-
RPD_OSP3	0.96%	2.10%	-0.40%			-0.03%	-4.63%	1.59%	
RPD_SP3	0.96%	2.10%	-0.40%			-0.03%	-4.63%	1.59%	
RPD_Di	1.31%	2.30%	-0.60%			-0.18%	-1.55%	0.30%	

Table 7 Normalized computation time in void reactivity calculation of each method with MET-1000.

S_NP	14.7
OSP_3P	6.4
SP_3P	6.2
DP	1

direct calculation results are exactly identical to the perturbation calculation results in all four reactors. The validity of SP_3P and OSP_3P calculation functions in CBZ was proven.

Secondly, the sum of $\phi^{0\dagger}$-scattering and $\phi^{2\dagger}$-scattering components given by the SP_3P method equals to the $\phi^{0\dagger}$-scattering component reactivity given by the OSP_3P method. This suggests that reactivity defined by the term having unclear physical meaning belongs to the scattering-component reactivity. This term can be eliminated by math manipulation. Therefore, the OSP_3P method is superior to the SP_3P method from the perspective of physical interpretation.

Thirdly, we observe a slight advantage of the SP_3P/OSP_3P method in Tables 3 to 6. These two methods show more accurate non-leakage component calculation capability compared with the DP method. Besides, computation time is reduced compared with the S_NP method. These results demonstrate the advantages of using SP_3 to calculate reactivity because this new method provides more accurate results with shorter computing time. Additionally, the advantage of the new methods is more obvious in middle-sized cores. The biases on the non-leakage component reactivity in middle-sized core calculations are less than those in the large-sized cores. Due to the smaller core size, the middle-sized core

has stronger neutron leakage than the large-size core does. Furthermore, the difference on biases between the SP_3P/OSP_3P and DP methods in MET-1000 problem calculation is larger than that in the MOX-1000 problem. This is because the MET-1000 core has a harder neutron spectrum than the MOX-1000 core (also harder than two large-sized cores) due to the use of metallic fuel.

At present, the SP_3P and OSP_3P methods underestimate the leakage component reactivity about $4\% \sim 5\%$, and this leads to the overestimation of net reactivity. One possible reason for this underestimation on the leakage component reactivity may relate to the treatment on the boundary conditions. The current SP_3P/OSP_3P method is developed based on the classic SP_3 theory without changing boundary conditions. The boundary conditions, however, have been systematically discussed by Y. Chao[3] in the advanced SP_3 theory. The authors believe that this underestimation on the leakage component reactivity can be reduced if the SP_3P/OSP_3P method is improved by the advanced SP_3 theory. This is a task for future study.

3.3. Local void pattern

The problem brought by the term having unclear physical meaning and the new methods verification were discussed in the last section. Next, applicable scenarios of the new methods are going to be discussed with a local void pattern problem.

As introduced at the beginning of Section 3.1, the reactor is modeled as a two-dimensional multi-layer (multi-ring) cylinder in the present work. Figure 1 depicts how the MET-1000 reactor is modeled in FRBurner as an example. The y-direction is axial direction, and the x-direction is radial direction. The width of each layer is calculated from the number of assemblies in each layer. Medium information corresponding to each cell according to number are listed in the right of the figure. Eleven media are used to describe the respective layers, and five of these are fuel medium for fuel layers (fuel as-

semblies). In this work, the fuel media in the same height are regarded as a plate. The local void pattern which is going to be discussed contains three cases: (1) the first plate is voided, (2) the third plate is voided, and (3) the axial-center region is voided. Since it is known that SP_3P gives exactly the same result as OSP_3P, only the result of OSP_3P will be discussed in this section.

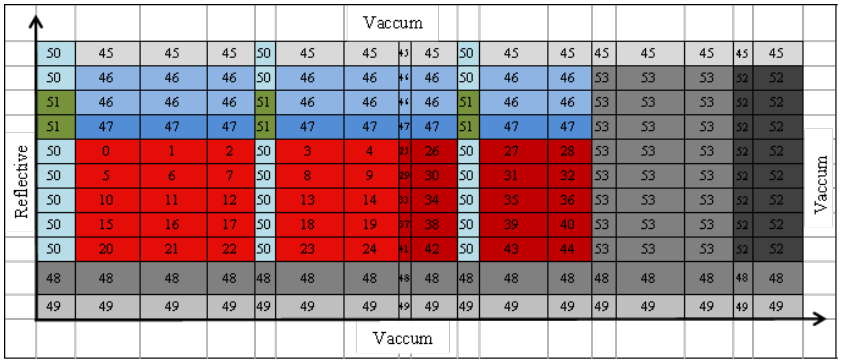

Number	Medium
0∼24	Inner core
25∼44	Outer core
45	Upper structure
46	Gas plenum
47	Replace sodium
48	Lower reflector
49	Lower structure
50	Empty duct
51	Control absorber
52	Shield rod
53	Radial reflector

Figure 1 Multi-layer cylinder model of MET-1000.

Figure 2 can represent the model of the core if we further simplify the schematic. The colored part represents voided region. The domainant neutron leakage components

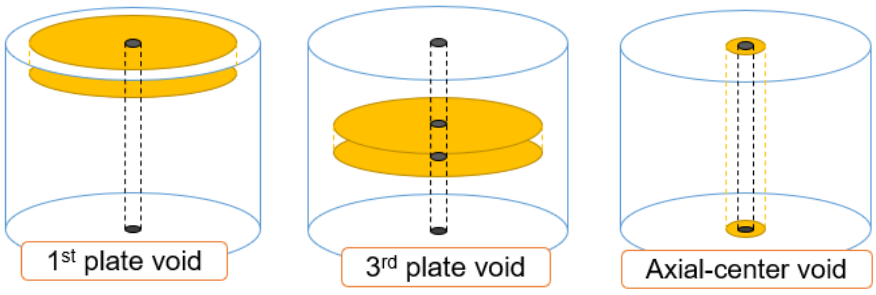

Figure 2 Local void pattern schema.

for these three void patterns are quite different since the gradients of neutron flux in these voided regions are different from each other. In the first-plate void pattern case, neutron leakage in both the axial- and radial-directions is dominant. In the third-plate void pattern, the axial-direction neutron leakage is suppressed, and the radial-direction neutron

leakage must be dominant. In the axial-center void pattern, the axial-direction neutron leakage must be dominant. We can investigate for which void pattern the OSP_3P method is more advantageous through these local void pattern problems which have different dominant leakage components.

The net, scattering, and leakage component reactivity given by the OSP_3P and DP methods are compared to those given by the S_NP method. The comparisons are summarized in **Figures 3** to **5**, and the corresponding data are summarized in Tables 8 to 10.

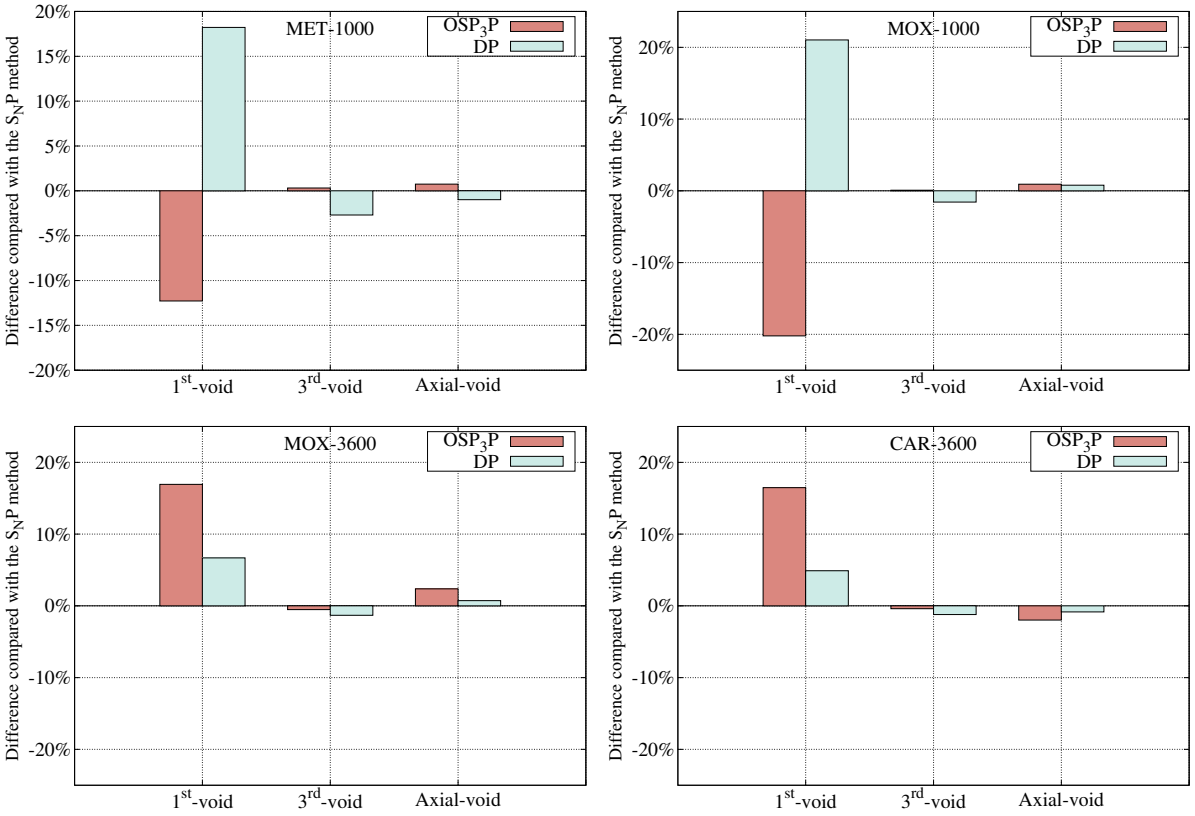

Figure 3 Net reactivity perturbation calculation of local void pattern.

Firstly, it seems that the SP_3P/OSP_3P method does not show any advantage for the net reactivity calculation (Figure 3). This is caused, however, by error cancellation with the DP method. The signs of non-leakage and leakage component reactivities are opposite. Therefore, there is error cancellation on net reactivity calculation, and this is one aspect of

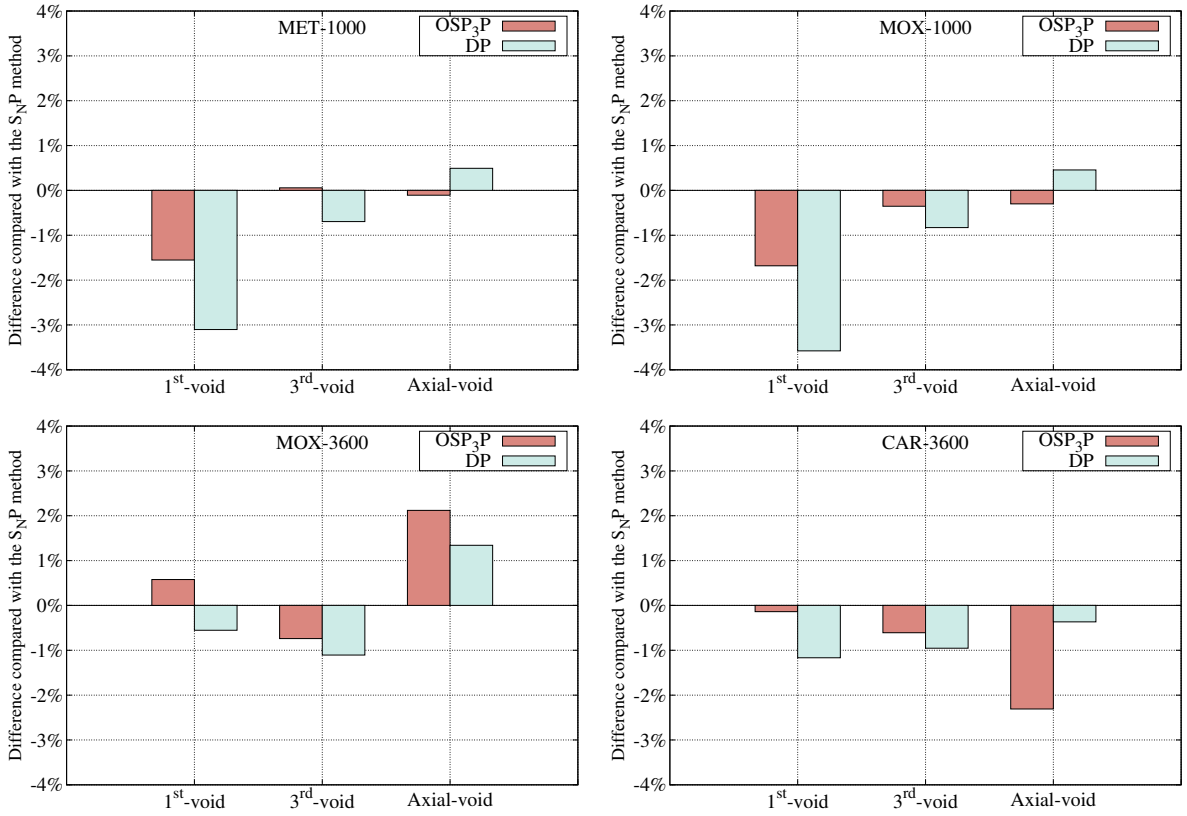

Figure 4 Scattering component reactivity perturbation calculation of local void pattern.

Table 8 Net reactivity perturbation calculation of local void pattern. [unit: pcm]

	1st-void			3rd-void			Axial-void		
	OSP_3P	DP	TP	OSP_3P	DP	TP	OSP_3P	DP	TP
MET-1000	-78.7	-89.8	-106.1	910.8	883.4	907.8	165.9	163.2	164.8
MOX-1000	-26.6	-40.3	-33.3	842.0	828.1	841.3	141.1	140.9	139.8
MOX-3600	89.5	81.8	76.7	785.1	778.9	789.2	58.4	57.5	57.0
CAR-3600	99.1	89.3	85.1	884.7	877.5	888.2	5.9	5.9	6.0

Table 9 Scattering component reactivity perturbation calculation of local void pattern. [unit: pcm]

	1st-void			3rd-void			Axial-void		
	OSP_3P	DP	TP	OSP_3P	DP	TP	OSP_3P	DP	TP
MET-1000	396.4	390.2	402.7	1052.1	1044.2	1051.5	212.7	214.0	213.0
MOX-1000	242.1	237.5	246.3	884.0	879.7	887.1	152.8	154.0	153.3
MOX-3600	240.1	237.4	238.7	722.1	719.4	727.5	59.8	59.3	58.6
CAR-3600	296.8	293.8	297.2	830.0	827.1	835.1	6.1	6.2	6.2

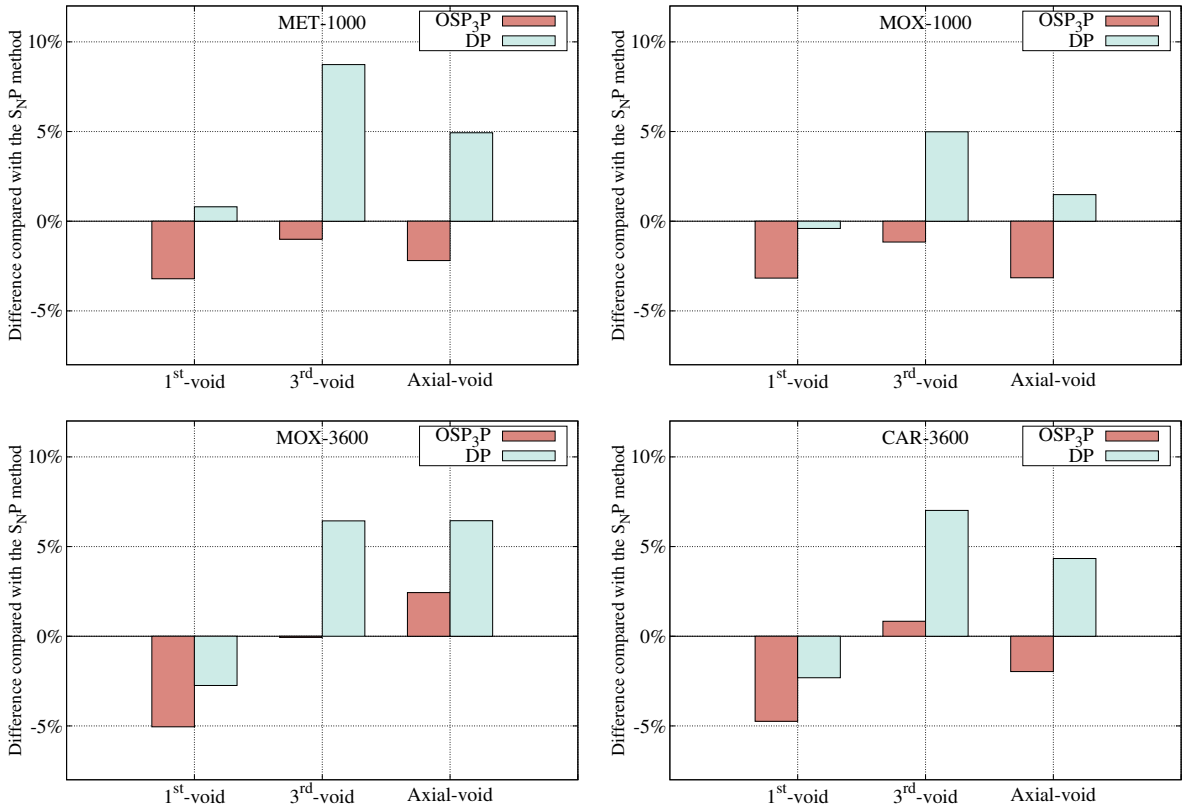

Figure 5 Leakage component reactivity perturbation calculation of local void pattern problem.

Table 10 Leakage component reactivity perturbation calculation of local void pattern problem. [unit: pcm]

	1st-void			3rd-void			Axial-void		
	OSP_3P	DP	TP	OSP_3P	DP	TP	OSP_3P	DP	TP
MET-1000	-497.9	-518.5	-514.4	-200.2	-219.9	-202.3	-59.6	-64.0	-61.0
MOX-1000	-299.6	-308.1	-309.4	-160.8	-170.8	-162.7	-34.7	-36.4	-35.9
MOX-3600	-190.5	-195.1	-200.6	-52.3	-55.7	-52.3	-12.1	-12.6	-11.8
CAR-3600	-247.2	-253.5	-259.5	-76.4	-81.1	-75.8	-1.2	-1.3	-1.3

the reason why reactivity must be decomposed. Naturally, the component-wise component reactivity should be paid more attention to.

Secondly, the following points can be summarized.

(1) The OSP_3P method shows merit on the scattering and leakage component reactivity calculations overall. This point can be explained with the characteristic of these two components of reactivity.

(2) The scattering component reactivity is significantly influenced by both forward and adjoint neutron fluxes. The peak of both fluxes occurs in the center of reactor. Consequently, the third-plate void pattern shows the largest scattering component reactivity. Although the scattering component reactivity has no direct relationship with the neutron flux gradient, the correlation between them can be revealed through a comparison of the first- and third-plate void patterns. There are two reasons for increase in neutron flux gradient for the first plate; one is the proximity to the edge, and the other is the presence of strong neutron absorber.

(3) The leakage component reactivity is significantly influenced by the changes in diffusion coefficient and the gradient of neutron flux. Comparing the first- and third-plate void patterns, the OSP_3P method predicts the leakage component reactivity for the region where the neutron leakage is not obvious.

(4) On the whole, the biases of new method results are less than those of DP method results.

It is necessary to point out that the center assembly of the MET-1000, MOX-1000, MOX-3600, and CAR-3600 cores are the secondary control assembly, the secondary control assembly, the center reflector, and the fuel assembly, respectively. For the secondary control assembly, the control absorber material exists beyond the active fuel region as shown in the benchmark report[7]. This is the reason for the significantly different behavior of axial-center void pattern calculation on the MOX-3600 and CAR-3600 cores.

Thirdly, the energy wise reactivity information would be helpful. Regarding the discussion above, only the scattering and leakage component reactivity of MET-1000 calculation are summarized in **Figure 6**. The left-hand-side figures show the scattering component

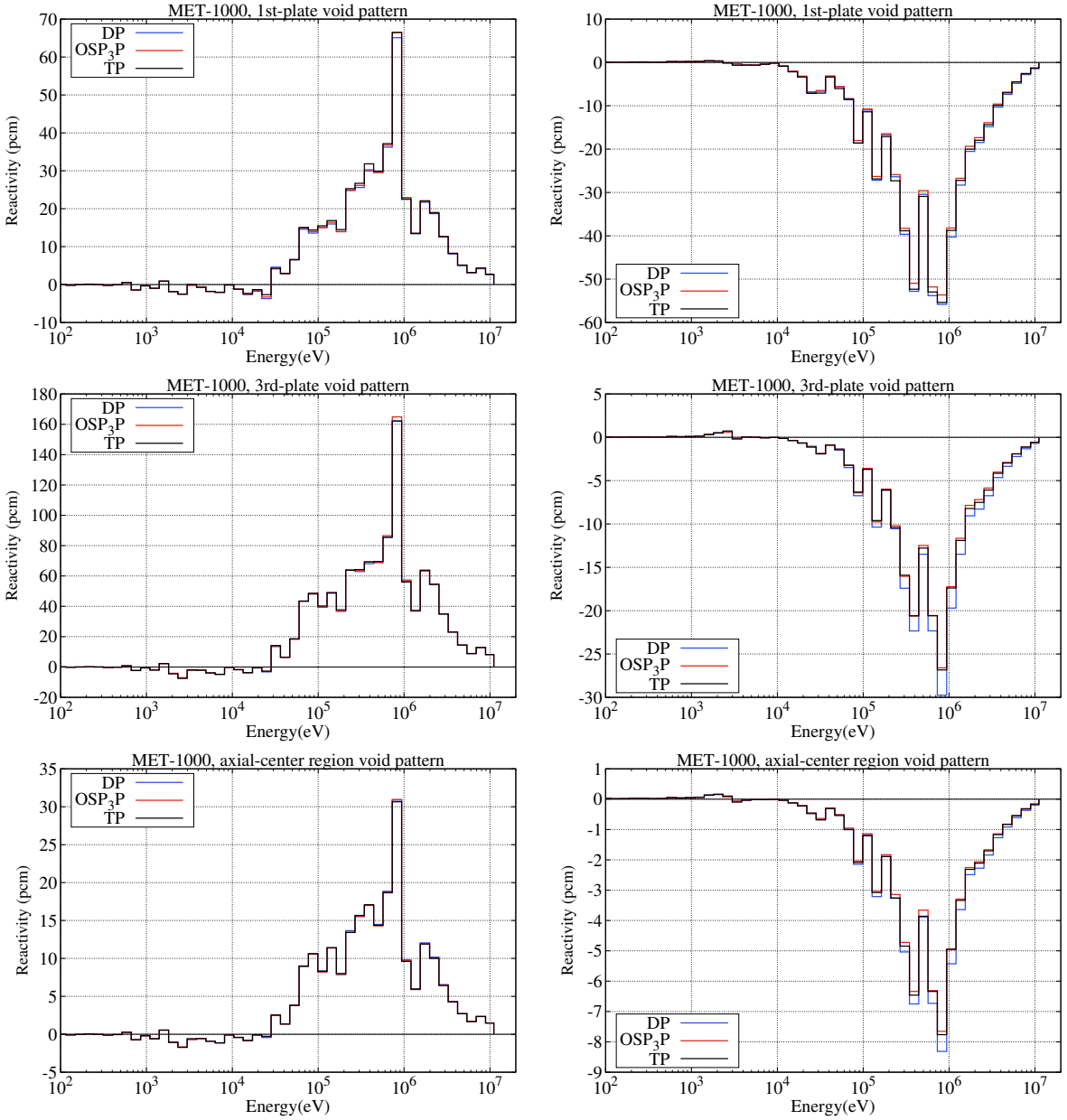

Figure 6 MET-1000 core local void pattern energy-wise reactivity comparison.

reactivity and the right-hand-side figures are the leakage component reactivity. It is notable that the DP method results display relatively larger bias on leakage component reactivity calculation for the third-plate void and axial-center region void patterns, while

the OSP_3P method yields more accurate results on the whole. For the scattering component reactivity, we can refer to a partial enlargement figure (Figure 7) for a clear view. The enlarged energy range is 10^5 eV to 10^6 eV since the reactivity in this energy range is higher than that in other ranges. Although the bias of each energy group is small, we can still say that the OSP_3P method yields a more accurate result for the scattering component reactivity in general. In particular, when the differences of bias on each energy group are summed together, the total difference is not negligible (as shown in Figure 4). Despite

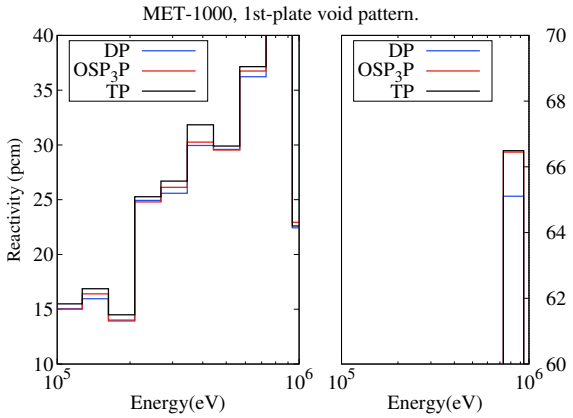

Figure 7 Partial enlargement of energy-wise scattering component reactivity, first-plate void case.

the magnitude of leakage component reactivity itself is not large, Figure 6 still presents the advantage of the OSP_3P method on the scattering and leakage component reactivity calculations. Meanwhile, the results displayed in the previous section reveal that the bias on leakage component reactivity of the DP method is less than that of the SP_3P method, which is opposite to the results shown in this section. This opposite point is the difference in the void pattern of calculations in these two sections. The whole core void pattern leads to a more significant neutron leakage. The local void pattern calculation results suggest that the neutron leakage of voided region affects the OSP_3P methods significantly. For the scattering component reactivity, the OSP_3P method shows merit when the neutron leakage is obvious. For the leakage component reactivity, the OSP_3P method shows merit when neutron leakage is not obvious.

Based on the calculations involved in the present work, we conclude that the SP_3P and OSP_3P methods show an advantage for void reactivity calculation if the neutron leakage is significant.

4. Conclusion

A new method, SP_3P (OSP_3P), for fast reactor reactivity analysis based on the SP_3 and perturbation theories is proposed in this work. This new method is verified through comparison with direct calculation and transport (S_N) perturbation calculation with four fast reactor concepts that differ from each other in fuel type and core size.

Firstly, the SP_3P results agreed with direct calculation results in all four fast reactor calculations, which suggests the equation derivation is correct and code implementation is successful. Compared with the biases of the DP method on the non-leakage component reactivity, the advantage of SP_3P method is obvious. Then, the SP_3P method can serve as a substitute for the DP method in fast reactor reactivity analysis considering the computing time and calculation accuracy.

Secondly, we resolved the difficulty in categorizing the $-\frac{2}{5}(\phi_{g'}^{2\dagger} - \phi_g^{2\dagger})\Delta\Sigma_{s,g'\to g}^0\phi_{g'}^{\prime 0}$ term by tracing its source. The sum of $\phi^{0\dagger}$-scattering and $\phi^{2\dagger}$-scattering components given by the SP_3P method equals to $\phi^{0\dagger}$-scattering component given by the OSP_3P method. This fact indicates that we resolved this difficulty properly.

Thirdly, three different local void pattern problems are used to illustrate the advantage of the SP_3P method. Based on the calculation result with designed void condition in the present work, the SP_3P method shows an advantage in the prediction of scattering component reactivity when the neutron leakage is relatively significant.

As for future work, it is possible that the current SP_3P method can be improved with the advanced SP_3 theory contributed by Chao[3]. In the work by Chao, the boundary condition is well-discussed. The authors believe that the SP_3P method can be further improved if the boundary condition is well-treated, and the advantage over the diffusion solver should become more obvious.

Acknowledgements

This work was supported by *MEXT Innovative Nuclear Research and Development Program*, grant number: JPMXDO219209423. Besides, this work was supported by *JST SPRING*, grant Number: JPMJSP2119 as well, since one of the authors (Jun-Shuang Fan) was supported by DX fellowship in Hokkaido University.

References

[1] Gelbard E. M. Application of spherical harmonics method to reactor problems. Pittsburgh (U.S.A): Bettis Atomic Power Laboratory; 1960, WAPD-BT-20.

[2] Larsen E. W., Morel J. E. and McGhee J. M. Asymptotic Derivation of the Multigroup P1 and Simplified PN Equations with Anisotropic Scattering. Nuclear Science and Engineering. 1996; Vol. 123:328-342.

[3] Chao Y.-A. A new and rigorous SP_N theory for piecewise homogeneous regions. Annals of Nuclear Energy. 2016; 96:112-125.

[4] Jeon S., Hong H., Choi N. and Joo H.-G. GPU acceleration of the prototype pinwise core analysis code VANGARD. ANS M&C 2021 (The International Conference on Mathematics and Computational Methods Applied to Nuclear Science and Engineering). 2021 October 3-7; Raleigh, North Carolina. doi=10.13182/M&C21-33727.

[5] Vidal-Ferràndiz A., González-Pintor S., Ginestar D., Demazière C., Verdú G. Pin-wise homogenization for SPN neutron transport approximation using the finite element method. Journal of Computational and Applied Mathematics. 2018; Volume 330: 806-821.
https://doi.org/10.1016/j.cam.2017.06.023.

[6] Pan Q.-Q., Zhang T.-F., Liu X.-J. and Wang K. SP_3-coupled global variance reduction method based on RMC code. NUCL SCI TECH 32, 122 (2021).
https://doi.org/10.1007/s41365-021-00973-0

[7] Stauff NE, Kim TK, Taiwo TA et al. Benchmark for neutronic analysis of sodium-cooled fast reactor

cores with various fuel types and core sizes. NEA-NSC-R-2015-9. Paris: OECD/NEA; 2016.

[8] Waltar A.E., Todd D.R., Tsvetkov P. V. (Eds.) Fast spectrum reactors. New York: Springer Science & Business Media; 2012. 125 p.

[9] Chiba G. and Endo T. Numerical benchmark problem of solid-moderated enriched-U-loaded core at Kyoto university critical assembly. J Nucl Sci Technol. 2019; Vol. 57:187-195.

[10] Tatsumi M. and Yamamoto A. Advanced PWR core calculation based on multi-group nodal-transport method in three dimensional pin-by-pin geometry. J Nucl Sci Technol. 2003; Vol. 40:376-387.

[11] Stamm'ler R. J. and Abbate M. J. Methods of steady-state reactor physics in nuclear design, vol. 111. Academic Press London, 1983.

[12] Fan J.-S. and Chiba G. Development and verification of fast reactor burnup calculation module FRBurner in code system CBZ. J Nucl Sci Technol. 2021; Vol. 58:1269-1287.